EFDA–JET–PR(12)04

M. Odstrcil, J. Mlynar, T. Odstrcil, B. Alper, A. Murari,
and JET EFDA contributors

Modern Numerical Methods for Plasma Tomography Optimisation

Modern Numerical Methods for Plasma Tomography Optimisation

M. Odstrcil[1,2], J. Mlynar[2], T. Odstrcil[1], B. Alper[3], A. Murari[4],
and JET EFDA contributors*

JET-EFDA, Culham Science Centre, OX14 3DB, Abingdon, UK

[1]Association EURATOM-IPP.CR, FNSPE, Czech Technical University in Prague, CZ-115 19, Czech Republic
[2]Association EURATOM-IPP.CR, Institute of Plasma Physics AS CR, v.v.i., Za Slovankou 3, CZ-182 00 Praha 8, Czech Republic
[3]EURATOM-CCFE Fusion Association, Culham Science Centre, OX14 3DB, Abingdon, OXON, UK
[4]Association EURATOM-ENEA sulla Fusione, Consorzio RFX, Corso Stati Uniti, 4, I-35127, Padova, Italy
** See annex of F. Romanelli et al, "Overview of JET Results", (23rd IAEA Fusion Energy Conference, Daejon, Republic of Korea (2010)).*

Preprint of Paper to be submitted for publication in
Nuclear Instruments and Methods in Physics Research Section A

ABSTRACT

Tomography of fusion plasmas is widely applied in order to improve knowledge of plasma emissivity distributions although it is challenging due to sparse spatial resolution of the measured plasma projections. An optimised version of robust and fast tomography algorithm based on Tikhonov regularisation constrained to Minimum Fisher Information is presented in this contribution. A new regularisation matrix enforcing preferential emissivity smoothness along magnetic flux surfaces is introduced. The paper also details application of advanced numerical methods leading to substantial decrease in computation time. Subsequent implementation of fast presolvers of the inverse problem further contributed to the algorithm efficiency and also improved stability of the tomography reconstruction. Finally, reliability and performance of the tomography algorithm is exemplified on reconstruction of soft X-ray data evolution following tungsten ablation into plasma of the JET tokamak. The resulting reconstruction speed is compared to other referenced tomography algorithms.

1. INTRODUCTION

Numerical methods for advanced data analyses have progressed to a qualitatively new level due to recent extensions of available numerical packages and libraries. This applies to both proprietary and open access languages (in our working experience MatLab and Python, respectively). A wide usage of the numerical libraries combined with object programming allows for a cleaner, more succinct implementation of the algorithms, and for numerical optimisation of the code performance.

In this article, potential of the advance will be exemplified on optimisation of the Minimum Fisher Regularisation (MFR) algorithm [1] including applications of MFR in the soft X-ray tomography at JET [2]. In general terms, plasma tomography aims at determining spatial characteristics of plasma emissivity from line-integrated measurements (plasma projections). Due to limited access, data on plasma projections are sparse so that plasma tomography typically presents an under determined problem, with rather modest spatial resolution. Even worse, tomography is a classical instance of the inversion tasks, which belong to so-called ill-posed problems. The ill-posed problems are challenging in particular due to their instability, i.e. high sensitivity to consistency of input data { a small data error in the projections can cause major artefacts in the resulting emissivity distribution. To achieve a unique and robust solution, some kind of regularisation process must be implemented in plasma tomography as well as sufficient a-priori information, for more details see [3].

Besides TCV and JET tokamaks, the MFR tomographic algorithm has been implemented also at TORE SUPRA in CEA France, COMPASS in IPP Prague [4] and GOLEM in CTU Prague [5]. Increasing interest in soft X-ray measurements at Joint European Torus JET presented substantial incentive for the optimisation work. soft X-ray tomography at JET is particularly challenging due to the experimental set-up, which is far from being dedicated to the tomography task. Spatially resolved information is collected by pin-hole cameras, which cover three toroidally separated plasma cross-sections, see Fig.1. Their toroidal separation hampers temporal resolution (fast processes, $t \lesssim 10\mu s$ cannot be considered toroidally symmetrical in tokamaks) as well as position reliability

of the reconstruction [6]. The horizontally oriented camera S4 is by 15.6° declined in the toroidal direction, and the spectral sensitivity of the vertical and horizontal cameras differs due to different thicknesses of the shielding beryllium foils.

On the other hand, JET provides world-wide unique data for fusion research. With major radius R=2.96m and minor radius a = 1.25m it is currently the biggest tokamak worldwide, and the only one capable of operation with tritium, the fuel component of the future fusion power reactors including the ITER facility. From 2011, JET is operating with the ITER-like, fully metal first wall (plasma facing components) made of beryllium and tungsten. Application of these materials, which are susceptible of enhancing plasma radiation losses, has led to increased interest in soft X-ray radiation measurements and analyses. This contribution demonstrates that optimised MFR tomography can disclose useful and reliable information on evolution of spatial distribution of the SXR radiation (the SXR emissivity evolution) in spite of the challenging diagnostic setup.

In Section 2, the pixel tomography method based on Tikhonov regularisation with iterative minimisation of the Fisher information is briefly presented. Section 3 is focused on optimisation of the reconstruction constrains, namely the anisotropic smoothness and the boundary conditions. Numerical amendments of the algorithm compared to the previous MFR versions [1], [7] also led to significant increase of the reconstruction speed without deterioration of the reconstruction quality. These amendments are detailed in Section 4. Finally, in Section 5, performance of the optimised MFR algorithm is exemplified on the re- construction of evolution of soft X-ray emissivity after tungsten ablation in JET Pulse No: 68373. A comparison of the optimised MFR reconstruction speed to the computation speed of other available plasma tomography algorithms is also provided.

2 MINIMUM FISHER INFORMATION METHOD

In the pixel tomography methods, the unknown two-dimensional (2D) emissivity cross-section g(x; y) is discretised to N values gj in finite number of pixels $j \in 1; ..., N$. In the emissivity reconstruction process, the unknown values of g_j are searched so that they t the measured projections, i.e. the line integrated data f_i.

After discretisation of the emissivity to the pixel grid, the problem can be rewritten as a set of linear equations

$$f_i = \sum_j^N T_{ij}\, g_j + \xi_i \quad i \in 1, ..., L \tag{1}$$

T_{ij} denotes the geometric (contribution) matrix, g_j is the emissivity in the j-th pixel, ξ_i represents data errors and L is number of detectors. This system of equations is ill-posed and in the case of fusion research diagnostic systems usually under determined (L < N). One of the methods that nd a trustworthy solution is the Tikhonov regularisation which minimises the reconstruction residual constrained to an object function (also known as the regularisation function) O(g):

$$\min_g \left(\| Tg - f \|^2 + \lambda O(g) \right) \tag{2}$$

where $\|Tg - f\|^2$ is quadratic mist (the residual), and λ is the regularisation parameter. The object function O(g) imposes some realistic a-priori information – the expected emissivity smoothness, entropy or probability distribution.

In this paper, the Minimum Fisher Information (MFI principle) acts as the object function due to advantages presented in [1] and also because of previous positive experience [7].

$$I_F = \int \sum_{i,j=1}^{2} \left| \frac{\partial g(x,y)}{\partial x_i} \frac{\partial g(x,y)}{\partial x_j} \frac{1}{g(x,y)} \right| dx\,dy \tag{3}$$

The MFI principle regularises eq. (2) by enforcing sufficient and physically relevant smoothness to the reconstructed image. Solution of the Tikhonov regularisation for a linear regularisation matrix H is

$$Ag = \left(\tilde{T}^T \tilde{T} + \lambda H \right) g = \tilde{T}^T \tilde{f} \tag{4}$$

Abbreviation $\widetilde{T}_{ij} = T_{ij}/\sigma_i$ and $\widetilde{f} = f_i/\sigma_i$ is used for convenience, where σ_i is standard deviation of the expected error in signal.

The regularisation parameter λ sets strength of the a-priori constraint on Fisher information I_F with respect to the value of the residual $\|Tg - f\|^2$. Underestimated value of λ results in over-fitting and the other extreme leads to over-smoothing. In order to determine a well-defined value of the regularisation parameter λ, the χ^2 criterion is applied as follows

$$\chi^2 = \sum_{i}^{L} \frac{1}{L} \left(\frac{T_{ij}\, g_j - f_i}{\sigma_i} \right)^2 \approx 1 \tag{5}$$

see [1], [3] for details.

The regularisation matrix H, which introduces a discretised and linearised MFI term (eq. 3), is implemented in the form

$$H^{(k)} = \sum_{l} B_l^T W^{(k)} B_l \tag{6}$$

W denotes weighting matrix $W_{ij}^{(k)} = \delta_{ij}/g_j^{(k-1)}$ and Bi denote matrices of the discrete derivatives, corresponding to the difference operator. In other words, due to non-linearity of the MFI principle, the $H^{(k)}$ matrix depends on emissivity g_j and the Tikhonov regularisation must be solved iteratively, see [1].

Consequently, the MFR algorithm consists of two nested cycles. The inner cycle interpolates and searches the root of equation (5), while the outer cycle optimises the weighting matrix W. Notice that eq. (4) has to be solved in each step of the inner cycle.

3. OPTIMISATION OF THE RECONSTRUCTION CONSTRAINS

The matrices of the discrete derivatives in eq. (6) can be used to add further a-priori information. In

particular, plasma emissivity gradients in tokamaks are expected to be low along magnetic field lines but may be steep across the field. Therefore, an anisotropic smoothing matrix H has been introduced

$$H = S(\eta)B_{\|}^{T} W B_{\|} + S(-\eta)B_{\perp}^{T} W B_{\perp} \tag{7}$$

where S(x) is the logistic sigmoid function. The weighting parameter can be chosen e.g. so that the smoothness is maximised [6]. In MFR, the anisotropic smoothness cannot be implemented via the second derivatives as in [2]. Instead, the matrix $B_{\|}$ is composed from the first derivatives in radial, horizontal and diagonal directions (see Fig. 2). Directions and weights are determined for each pixel in the grid from unambiguous decomposition of magnetic flux surfaces to one parallel and one diagonal direction. The resulting matrix of discrete derivatives proved to cause artificial spiral patterns in reconstruction if high value of was used. However, this was fixed by symmetrisation of each discrete derivative – simply put, an opposite direction of the derivative was added to each pixel. The complementary matrix $B_{\perp}$ is then set to be perpendicular to $B_{\|}$ in each pixel.

A correction to finite width of chords (viewing lines) in geometric matrix was also used. In this amendment, every experimental chord with its angular view is decomposed to many linear subchords with weights corresponding to the level of the channel sensitivity in the direction. In the final geometric matrix T_{ij}, the effects of all subchords are averaged to the corresponding chord (i.e. into the matrix raw). The geometric matrix then correctly reflects finite widths and divergences of the real chords. As expected [3], this improvement had rather little but positive effect on the resulting reconstruction.

Boundary conditions – including non-negativity of plasma emissivity and its zero level outside the plasma edge – present another important instance of the available a-priori information. Implementation of the boundary conditions considerably helps to cope with sparse data. In the iteration process, any negative value is set to zero. In order to avoid subsequent divergence of the weighting matrix, its maximum value is set as follows

$$W_{ij} = \delta_{ij}/g_j \qquad g_j > \in$$
$$W_{ij} = \delta_{ij}/\in \qquad g_j \geq \in$$

where $\in$ is a pre-set small number. This formula constrains reconstruction to be at in non-positives values. In order to enforce the zero level outside the plasma edge, virtual chords are set to observe zero emissivity there. For this purpose, the edge is typically defined by position of the last closed flux surface, i.e. the plasma separatrix, and one virtual chord is set for each pixel outside this boundary.

4. SPEED OPTIMISATIONS

4.1 RECONSTRUCTION SPEED

The anisotropic smoothing matrix presented in Section 3 substantially improved the reconstruction performance (in particular, the convergence ameliorated), however it is an impediment to the

reconstruction speed. Indeed, the matrix elements can not be precalculated and xed constant since they depended on position and evolution of magnetic flux surfaces. In this respect, the advanced rapid methods such as generalised eigenvalues [2], generalised SVD or QR decomposition [8, 9] have no advantage over MFR in solving eq. (4). These methods require smoothing matrix H as defined in eq. (7) to remain constant; they rely on pre-solved decompositions of the system with which they can nd solution almost instantly. The only prospective for these rapid alternatives to MFR would be to apply a single weighting and smoothing matrix averaged over all required time frames as in the rapid version of MFR [7].

Another issue of the MFR with respect to the computation time is its non-linearity. Non-linear methods like MFR should be used for separate reconstruction in every time step and the corresponding matrices cannot be reliably determined and decomposed in advance. This implies that the lower limit for duration of one step in the MFR iteration is set by one full decomposition of matrix A according to eq. (4). This limit has been determined for a single core 1.7 GHz processor, image resolution 3520 pixels and Cholesky decomposition (see below) to equal approximately 40 ms. The decomposition required up to 90% of the total reconstruction time.

The reconstruction speed can be improved by decreasing resolution (number of pixels N), however, at some point this results in loss of information and degradation of the reconstruction quality. Lower resolution can be still used with advantage for the initial pre-solution of the emissivity shape $g^{(0)}$ for eq. 6, because a correct initial form of emissivity decreases the amount of subsequent iterations. Another option to get the initial shape $g^{(0)}$ is to use the rapid version of MFR [7], SVD or QR methods as a rapid pre-solver. This strategy resulted in significantly improved convergence and reconstruction speed.

For improved convergence and stability of the algorithm, it is also recommended to use logarithmic substitution for λ and χ^2 (log-log scale) in search of the root of eq. (5). This practice decreases the number of iterations required to solve eq. (4), which further decreases the computation time.

4.2 MATRIX INVERSION

Speed of the reconstruction is directly dependent on choice of suitable numerical tools for matrix operations. To start with, the matrix A in the eq. (4) is positive definite for $\lambda > 0$ and it is also sparse. Density of the matrix is usually a few percent, therefore the speed of matrix multiplication and inversion can be significantly improved if numerical recipes for sparse matrices are applied. A commonly recommended non-iterative algorithm for operations on sparse positive definite matrices is the Cholesky decomposition. In the MFR algorithm, the Cholesky decomposition is applied as it is implemented in the ANSI C library CHOLMOD. The CHOLMOD library uses sparse Cholesky factorisation based on dynamic supernodes [10] and the library allows to use updating/downdating of pre-solved Cholesky decomposition.

The basic principle of the updating/downdating relies in a possibility to add or subtract a low-rank matrix C in the form C^TC to the already decomposed matrix D:

$$\tilde{D} = D \pm C^T C \tag{8}$$

This equation can be solved quickly provided that nonzero pattern of the matrix $\tilde{D}$ remains unchanged. The condition is satifised in the case of the MFR method, if we denote

$$D = 1/\lambda_0 T^T T + H \tag{9}$$

and

$$C(\lambda) = \sqrt{\left|\frac{1}{\lambda_0} - \frac{1}{\lambda}\right|} T \tag{10}$$

The final form of the equation is then

$$(D \pm C^T C)g = Tf/\lambda \tag{11}$$

Speed-up of one step using update/downdate principle compared to full Cholesky decomposition is approximately from 10 for high resolution of 2000 pixels to 3× for low resolution of 500 pixels. Still, at least one full decomposition has to be performed in every outer cycle, and there are typically three outer cycles per reconstruction; two cycles may prove sufficient with a good pre-solution of g^0.

Iterative methods for operations on sparse positive definite matrices have been also tested, however only the Conjugate Gradient Method with incomplete sparse Cholesky decomposition and with the best choice of parameters would achieve speed competitive to the above detailed method.

5. EXPERIMENTAL RESULTS

The optimised code has been applied for analyses of JET soft X-ray (SXR) data from cameras S4 and V, see Fig. 1. In this section, the MFR performance is demonstrated on studies of SXR emissivity evolution after tungsten ablation in JET Pulse No: 68373. A standard resolution of 6840 pixels was used, corresponding to a mesh of 5cm × 5cm square pixels covering complete poloidal cross-section of the JET chamber.

As mentioned in the introductory Section 1, the horizontal and vertical cameras have slightly different spectral sensitivities owing to different thicknesses of their beryllium shielding foils: 350μm and 250μm, respectively. As a consequence, there is a minor inconsistency between horizontal and vertical data with respect to the tomographic reconstruction. In the first approximation, data correction can be done by re-normalisation of the total SXR emissivity so that it is equal for the two cameras. To this effect, the normalisation factor is to be determined before each tomographic reconstruction in the form of a ratio of horizontally and vertically observed SXR emissivities. For the ratio is due to slightly different spectral sensitivities of the two cameras, it is subject to rather rapid changes within plasma experiments depending on the evolution of plasma temperature and its

impurity contents, which is demonstrated in Fig.3. In this figure, ratio of the two total emissivities was determined by comparison of two separate emissivity reconstructions, first run on data from horizontal camera S4 only and second on data from vertical camera V only. For this purpose, poloidally symmetrical one-dimensional (1D) reconstruction – commonly referred to as the Abel Inversion [3] – was initially proposed, however, the MFR 2D tomography with anisotropic smoothing proved to provide a simpler and a more stable tool than the Abel Inversion, with lower dependency on correct positioning of the magnetic flux surfaces.

Another proposed method for iterative determination of the correction ratio is based on maximisation of the smoothness of the reconstructed emissivity gHg, see Fig.3. This method proved efficient in validation of the above described procedure and, besides, it can quantify consistency of the data. It can also provide a more reliable value of the ratio in case the prole is hollow or strongly asymmetric. However, compared to the direct MFR reconstruction for individual cameras it is slow and less stable.

In Figure 3, the evolution of ratio of the MFR reconstructed emissivities from separate horizontal and vertical cameras clearly demonstrates substantial change in spectral composition of plasma soft X-ray radiation following tungsten ablation in the JET Pulse No: 68373. The ratio decreases by as much as 35% during the impurity in flux. It is concluded that diffusion of the heavy impurity into the plasma results in increased radiation levels of soft X-ray radiation for energies around 3keV. At these energies the absorption factor of the 350μm beryllium shielding foil of the horizontal camera S4 is considerably higher that the absorption factor of the 250μm Be shielding foil of the vertical camera V. Similar abrupt changes of the ratio have been observed also during major sawtooth crashes.

It is to be underlined that without implementing this correction factor, the soft X-ray tomography at JET often results in non-convergence, in other words, no consistent solution is found within the expected errors σ_i, see eq. (4). Indeed, in Fig.3 it has been demonstrated that the error due to the different spectral sensitivities can be by an order of magnitude higher that the expected data error, which is typically about 3%-4%.

The MFR emissivity evolution after tungsten ablation in the JET Pulse No: 68373 with the correction factor and anisotropic smoothness is then straight-forward and very robust. The emissivity at time t = 15.035s is shown in Fig.4 and time evolution of poloidally averaged emissivity prole with subtracted background (initial) emissivity is presented in Fig.5. Figure 4 clearly demonstrates that the emissivity prole is hollow and not symmetrical. Therefore, application of the Abel Inversion which assumes full poloidal symmetry would not be appropriate. On the other hand, even with the observed 2D features it is possible to extract – if and when required – 1D emissivity prole in the form of poloidally averaged emissivity as shown in Fig. 5. In this figure, the emissivity prole is averaged along magnetic flux surfaces as imported from the JET routine magnetic reconstruction. Compared to the more widespread 1D Abel inversion, this procedure has two substantial advantages:

1. In the Abel inversion the geometric matrix in eq. 1 strictly requires correct positioning of magnetic flux surfaces, in particular in the plasma core. In contrast, the 2D MFR implements

the magnetic flux surfaces at the level of the anisotropic smoothing matrix only, in eq.7, so that errors in their positioning have only secondary effect on the reconstruction quality.

2. In the case of real 2D features (poloidal asymmetries) in plasma emissivity like in Fig.4 the Abel inversion may produce artefacts or need not converge at all.

The observed asymmetry of the heavy impurity radiation in figure 4 is in agreement with results published for the nickel injection in [2] where centrifugal force due to toroidal plasma rotation induced by NBI heating is referred to as the cause of the asymmetry. Indeed, in the JET Pulse No: 68373 neutral beam heating was applied at the level of 8.9MW during the tungsten ablation. As a matter of fact, in the case of tungsten ablation the asymmetry is well pronounced and can be identified even in raw data.

It is also worth noticing that given the sparse spatial resolution of the line-integrated measurements, the hollow prole would not be recognised without implementing the anisotropic smoothing according to Section 3. Furthermore notice that in Fig.5, the reconstruction with substracted background is slightly negative in the plasma centre around 55.02s. This is likely to be caused by cooling of the plasma by impurity radiation, combined with the heat transport from the core to outer regions. Quantitative studies of the heat and impurity transport would require sophisticated modelling, which is beyond the scope of this paper but it clearly indicates prospective applications for the MFR reconstruction analyses.

Finally, the reconstruction speed of the optimised MFR algorithm was compared to performance of similar numerical methods suitable for tomography reconstruction. The results are presented in table 1. Although the values of reconstruction speed from different references cannot be explicitly compared as the conditions were not identical, the pixel resolutions and CPU speed were similar.

CONCLUSION

In this paper, optimisation of the Minimum Fisher Regularisation algorithm including implementation of modern numerical methods is presented. The reconstruction quality and reliability was reinforced in particular by introduction of an anisotropic smoothing matrix. Computation speed increased, among others, due to rapid pre-solving procedures and an improved root searching process. Fast non-iterative solver for sparse matrices also significantly improved stability and speed of the tomographic reconstruction. Performance of the code was exemplified on analyses of the soft X-ray radiation data from tungsten ablation. Incompatibility of data due to different spectral sensitivities of the applied soft X-ray cameras was successfully corrected and evolution of non-symmetrical, hollow and strongly peaked soft X-ray impurity radiation was clearly identified. This demonstrates that the optimised MFR method provides a rapid, reliable and robust tool for experimental analyses of plasma emissivity even in rather challenging conditions.

ACKNOWLEDGEMENT

This work, supported by GA CR grant P205/10/2055 and MSMT grant LG11018, and the European

Communities under the contract of Association between EURATOM, IPP.CR, CCFE and ENEA, was carried out within the framework of the European Fusion Development Agreement. The views and opinions expressed herein do not necessarily reflect those of the European Commission.

REFERENCES

[1]. M. Anton, H. Weisen, M.J. Dutch, W. Linden, F. Buhlmann, R. Chavan, B. Marletaz, P. Marmillod, and P. Paris. X-ray tomography on the TCV tokamak. Plasma Physics and Controlled Fusion, **38**:1849, 1996.

[2]. L.C. Ingesson, B. Alper, H. Chen, A.W. Edwards, G.C. Fehmers, J.C. Fuchs, R. Giannella, R.D. Gill, L. Lauro-Taroni, and M. Romanelli. Soft X-ray tomography during ELMs and impurity injection in JET. Nuclear Fusion, **38**:1675, 1998.

[3]. L.C. Ingesson, B. Alper, B.J. Peterson, and J.-C. Vallet. Tomography Diagnostics: Bolometry and Soft X-Ray Detection. Fusion Science and Technology, **53**:528, 2008.

[4]. V. Weinzettl, D.I. Naydenkova, D. Sestak, J. Vlcek, J. Mlynar, R. Melich, D. Jares, J. Malot, D. Sarychev, and V. Igochine. Design of multi-range tomographic system for transport studies in tokamak plasmas. Nuclear Instruments and Methods Physics Research, Sect. A, **623**(2):806, 2010.

[5]. V. Svoboda, E. Bromova, I. Duran, O. Grover, J. Kocman, T. Markovic, M. Odstrcil, T. Odstrcil, O. Pluhar, J. Stöckel, A. Sindlery, G. Vondrasek, and J. Zara. The GOLEM Tokamak for Fusion Education. Contributed Papers 38th European Physical Society Conference on Plasma Physics, Eu- rophysics conference abstracts, 35G:P1.021, 2011.

[6]. J. Mlynar, M. Odstrcil, M. Imrisek, B. Alper, C. Giroud, A. Murari, and JET EFDA Contributors. 2D tomography of SXR data from toroidally separated cameras for studies of impurity injection and fast instabilities on JET. Contributed Papers 38th European Physical Society Conference on Plasma Physics, Europhysics conference abstracts, 35G:P4.052, 2011.

[7]. J. Mlynar, S. Coda, A. Degeling, B.P. Duval, F. Hofmann, T. Goodman, J.B. Lister, X. Llobet, and H. Weisen. Investigation of the consistency of magnetic and soft X-ray plasma position measurements on TCV by means of a rapid tomographic inversion algorithm. Plasma Physics and Controlled Fusion, **45**:169, 2003.

[8]. G.C. Fehmers, L.P.J. Kamp, and F.W. Sluijter. An algorithm for quadratic optimization with one quadratic constraint and bounds on the variables. Inverse problems, 14:893, 1998.

[9]. N. Terasaki, Y. Hosoda, M. Teranishi, and N. Iwama. Linear algebraic algorithms for high speed and stable reconstruction of plasma image. Fusion Engineering and Design, **34**:801–804, 1997.

[10]. Y. Chen, T.A. Davis, W.W. Hager, and S. Rajamanickam. Algorithm 887: CHOLMOD, supernodal sparse Cholesky factorization and up-date/downdate. ACM Transactions on Mathematical Software (TOMS), **35**(3):1–14, 2008.

[11]. J. Kim, S.H. Lee, and W. Choe. Comparison of the three tokamak plasma tomography methods for high spatial resolution and fast calculation. Review of Scientific Instruments, **77**:10F513, 2006.

[12]. T. Craciunescu, G. Bonheure, V. Kiptily, A. Murari, I. Tiseanu, V. Zoita, and JET EFDA Contributors. A comparison of four reconstruction methods for JET neutron and gamma tomography. Nuclear Instruments and Methods Physics Research, Sect. A, **605**:374{383, 2009.

Method	**Reference**	**CPU time [s]**
optimised MFR	this paper	0.2
MFR	[11]	1
Fast MEM	[11]	1.3
PTM	[11]	2.3
ML	[12]	210
ME	[12]	480–720
TR	[12]	48
MCBP	[12]	360

Table 1: Comparison of reconstruction time for different algorithms. The spatial resolution in ref. [12] and in the optimised MFR is 3520 pixels = 700 pixels, while in ref. [11] it is 4515 pixels = 675 pixels.

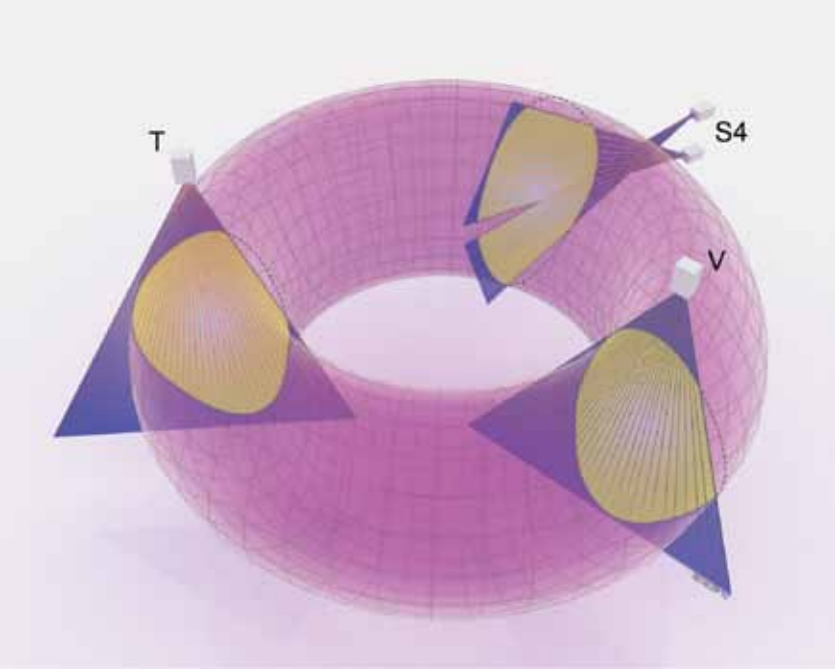

Figure 1: Experimental set-up of the soft X-ray cameras at JET.

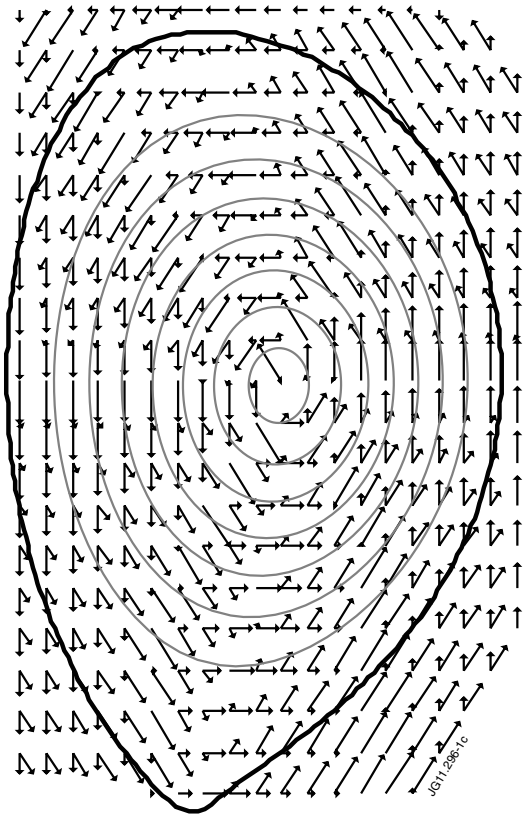

Figure 2: Decomposition of magnetic flux surfaces to diagonal and parallel directions in a finite set of rectangular pixels.

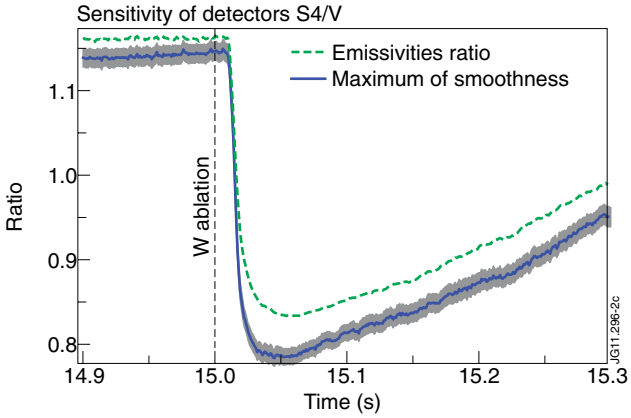

Figure 3: Change of emissivity ratios for cameras S4 and V in the JET Pulse No: 68373, following the tungsten ablation at t = 15s. The maximum of smoothness is plotted with estimated error.

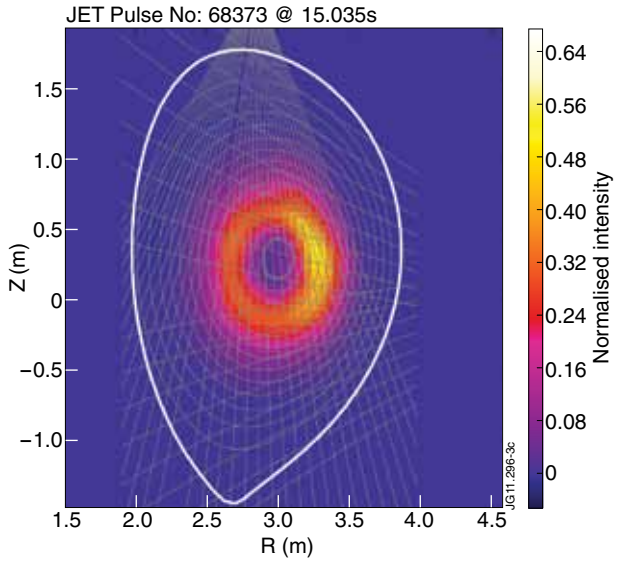

Figure 4: Reconstruction of the soft X-ray emissivity of the JET Pulse No: 68373, 35ms after the tungsten ablation. The colorbar is normalised to the peak intensity.

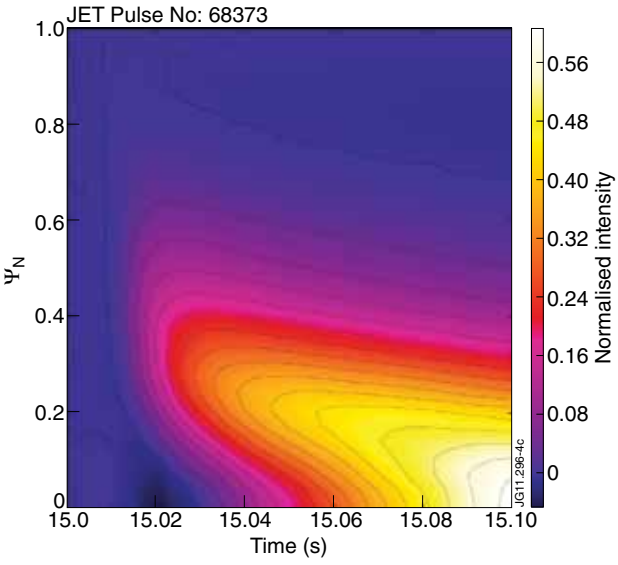

Figure 5: Time evolution of perturbation of the soft X-ray emissivity prole in JET Pulse No: 68373 following tungsten ablation. N denotes normalised magnetic flux (N = 0 at the magnetic axis, N = 1 at the plasma separatrix). The colorbar is normalised to the peak intensity.